ABE

Agricultural and Biological Engineering

https://ph04.tci-thaijo.org/index.php/abe/index

Published by the Faculty of Engineering, Khon Kaen University, Thailand

Rainfall intensity analysis for radar rainfall evaluation in the composite area of Takhli and Sattahip radar

Ratchawatch Hanchoowong[1]* and Siwa Kaewplang[2]

[1]Department of Civil Engineering, School of Engineering and Industrial Technology, Mahanakorn University of Technology, Bangkok, 10530, Thailand
[2]Department of Civil Engineering, Faculty of Engineering, Mahasarakham University, Maha Sarakham, 44150, Thailand

*Corresponding author.
Email address: rhanchoowong@gmail.com
doi: 10.14456/abe.2026.2

Received 19 November 2025
Revised 21 December 2025
Accepted 29 December 2025

Abstract
This study collected data on a total of 510 rain events between February 2018 and November 2020. It includes hourly rainfall data (R) from 238 ground-based automated telemetry stations and radar reflectivity data (Z) under a measurement radius of 240 km from Takhli and Sattahip radars. The Z-R relationships of Takhli radar and Sattahip radar were determined and applied to evaluate radar rainfall intensity in the composite area of these radars. The radar rainfall intensity in the composite area was analyzed using five methods: the rainfall intensity from (1) $Z = 138R^{1.6}$ (only Takhli radar), (2) $Z = 170R^{1.6}$ (only Sattahip radar), and the composite rainfall intensity from (3) $Z = 200R^{1.6}$ (Marshall and Plamer), (4) $Z = 300R^{1.6}$ (Woodley and Herndon), and (5) $Z = 138R^{1.6}$ and $Z = 170R^{1.6}$ (Takhli and Sattahip radar). These results were compared with the ground-based station data to determine the best method for evaluation based on the least statistical values, i.e., Root Mean Squared Error (RMSE), Mean Absolute Error (MAE), and BIAS. The results show that the composite results from Takhli and Sattahip radar were the most accurate, and this case can increase the accuracy compared to the 1st to 4th method by 22.26%, 10.25%, 3.89%, and 18.02% of the RMSE; 29.75%, 23.14%, 14.88%, and 14.88% of the MAE; and 361.54%, 42.31%, 100.00%, and 369.23% of the BIAS value, respectively.

Keywords: Radar reflectivity, Takhli radar, Sattahip radar, Rainfall intensity, Automated telemetry station

1. Introduction

Thailand frequently experiences flooding, particularly in the Eastern, Western, and Central regions, which receive water flowing from the high mountains in the North. This is also compounded by drought. This is due to a lack of proper and systematic water resource management. Water resource management requires accurate data showing rainfall volume and distribution both spatially and temporally. Therefore, traditional rain gauge stations with a resolution of only 200 cm^2 [1] are used, and in areas without rain gauges, such as deep forests, mountainous areas, and remote areas, this lacks accurate spatial rainfall data for water management.

Currently, remote sensing technology using weather radars is popularly used for rainfall measurement. The radar can continuously detect rainfall as soon as it reaches an area within the radar's detection radius. It also provides high-resolution spatial rainfall measurements, both spatially and temporally [2-7]. Therefore, combining spatial rainfall data from weather radars with rainfall data from ground-based rain gauge stations for rainfall assessments will significantly increase the accuracy of spatial rainfall estimates obtained from radars [8-9].

However, since weather radars do not directly measure rainfall, they transmit electromagnetic waves to measure rainfall. After these waves strike raindrops, they are reflected back to the radar receiver and converted to radar reflectivity (Z (mm^6/m^3)). This radar reflectivity varies depending on the size and distribution of raindrop particles (rain drop size distribution) within a given volume of atmosphere. When using radar reflectivity data to assess rainfall, These data were converted to rainfall intensity data (R (mm/h)) using the appropriate Z-R relationship equation ($Z=aR^b$) for the study area [10-15]. When applied to rainfall assessments in conjunction with rainfall data measured at rain gauge stations, the accuracy of rainfall estimates significantly increased. Furthermore, this study aimed to improve the accuracy of radar rainfall estimates in the composite area of the Takhli and Sattahip radars.

This study therefore applied the appropriate Z-R relationship equation for the Takhli and Sattahip radars to the combined rainfall estimates to obtain radar rainfall intensity values in the composite area, which were more accurate than those estimated using the Z-R relationship equation for either the Takhli or Sattahip radars alone.

2. Materials and methods

2.1 Data study

The composite area of the Takhli and Sattahip radars is within the 240 km detection radius of the Takhli and Sattahip radars as shown in Figure 1.This study collected rainfall events that occurred within a 240 km measurement radius of the Takhli Royal Rainmaking Radar Station, S-band dual polarization type, which measured every 6 minutes from 14 measured elevation angles, namely 0.5°, 1.3°, 2.3°, 3.4°, 4.7°, 6.2°, 7.9°, 9.8°, 12.1°, 14.7°, 17.7°, 21.2°, 25.2°, and 29.8°, respectively, during August 2018 to November 2020, and the Sattahip Royal Rainmaking Radar Station, S-band Doppler type, which measured every 6 minutes from 14 measured elevation angles, namely 0.5°, 1.5°, 2.4°, 3.4°, 4.3°, 5.2°, 6.2°, 7.5°, 8.7°, 10.0°, 12.0°, 14.0°, 16.7°, and 19.5°, respectively, between February 2018 and November 2020. Radar reflectivity (Z) data were stored in volume files and rainfall data from the Hydro-Informatics Institute (HII)'s ground-based automatic telemetry station. Each rainfall event used in the study required consistent radar and ground-based automatic telemetry data. Both data were quality checked and error-corrected before being used in the study.

This study examined data quality and adjusted for errors in the Takhli and Sattahip radar reflectivity data, which were affected by ground clutter caused by radar beams clashing with permanent reflectors (ground clutter), such as mountains, buildings, or other structures. These objects, which are not rain clouds, resulted in data inaccuracies.

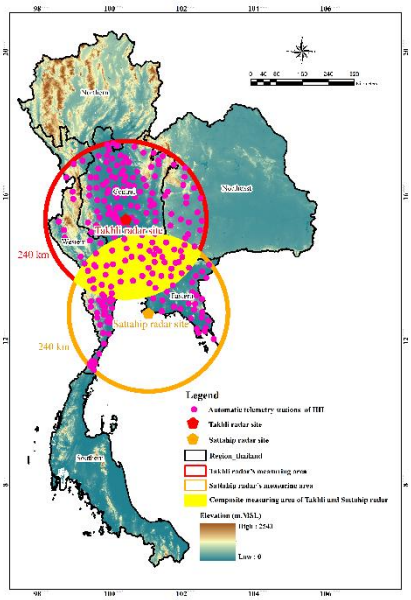

Figure 1 Composite area of radars within a 240 km detection radius of the Takhli and Sattahip radars

The measured radar reflectivity values. To correct for ground clutter errors for this study, a Ground Clutter Map was created. The radar reflectivity values in the ground clutter locations were adjusted by calculating the reflectivity values of adjacent pixels using the interpolation method [16-17]. Regarding the impact of radar beams striking permanent reflectors, which resulted in lower-than-normal radar reflectivity values in areas behind obstacles, this study adjusted the reflectivity values by considering the radar reflectivity values from monthly accumulated rainfall measurements to determine the location of beam blockage. The radar reflectivity values of the pixels in the beam blockage locations were adjusted by calculating the radar reflectivity values of adjacent pixels using the interpolation method. Interpolation [16-17], while attenuation is affected by radar energy as it travels through atmospheric gases, water vapor, oxygen, and rainfall [18-19], the radar energy is absorbed and attenuated. The sensitivity of a radar signal to energy attenuation depends on the transmitted radar wavelength. Energy attenuation is a problem for X-band and C-band radars, which have wavelengths of 2.5 and 5.5 cm, respectively, but not for S-band radars with wavelengths of 10.7 cm [20]. Therefore, the Takhli and Sattahip radars, which are S-band radars, are not affected by attenuation. To avoid radar reflectivity, only radar reflectivity data greater than 15 dBZ is used to detect signals not caused by rain clouds. To avoid radar reflectivity, hail signals are detected. Therefore, if the radar reflectance value is greater than 53 dBZ, it will be considered equal to 53 dBZ [21]. The reflectance data from the Takhli and Sattahip radars, after adjusting for errors from 14 different measurement angles, were selected to determine the optimal measurement angles for the Takhli and Sattahip radars. The measurement angles provided rainfall coverage within the Takhli radar's measurement radius. The Sattahip radar, combined with its ability to measure rainfall closest to that measured by ground-based telemetry stations, also had the lowest error after adjustment.

The radar reflectance values due to ground clutter and beam blockage remained minimal. The results of the examination of the optimal measurement angles for the Takhli and Sattahip radars show examples of the three measurement angles that measured closest to the ground. As shown in Figures 2 and 3, it was found that measuring angle 1 (Takhli radar is 0.5°, Sattahip radar is 0.5°), which is the lowest measurement angle, still experienced problems due to significant beam blockage. Considering measurement angle 2 (Takhli radar is 1.3°, Sattahip radar is 1.5°), it can be seen that the beam blockage problem has decreased, and rain clouds can still be detected covering the area within the radar station's measurement radius. While considering the 3rd measurement angle (Takhli radar is 2.3°, Sattahip radar is 2.4°), the rain cloud covered less area under the measurement radius of the radar station compared to the 2nd measurement angle (Takhli radar is 1.3°, Sattahip radar is 1.5°). For the aforementioned reasons, when considering the quality of the radar wave reflectivity data, after adjustment, the error values caused by Ground Clutter and Beam Blockage must be minimized. And the rain cloud must cover the area under the measurement radius of Takhli radar and Sattahip radar stations as much as possible compared to other measurement angles. Therefore, the radar wave reflectivity data from the 2nd measurement angle (Takhli radar is 1.3°, Sattahip radar is 1.5°) is the most appropriate measurement angle for Takhli radar and Sattahip radar.

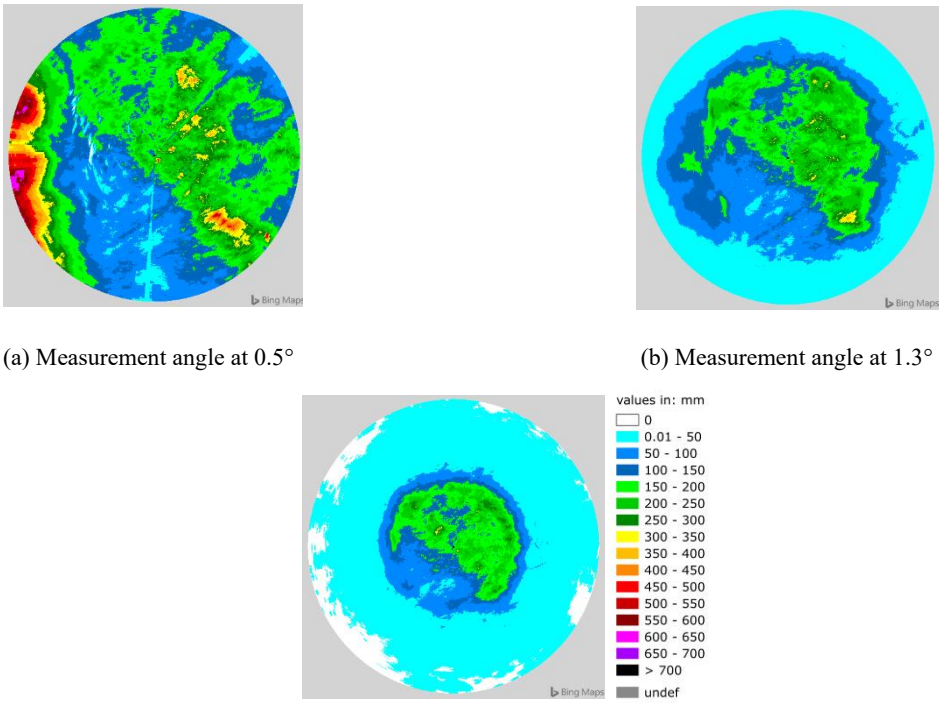

(a) Measurement angle at 0.5° (b) Measurement angle at 1.3°

(c) Measurement angle at 2.3°

Figure 2 Sample area of monthly accumulated rainfall measured by Takhli radar from 3 elevation angles of the August 2019 rainfall event

This study examined the quality of hourly rainfall data from ground-based automatic telemetry stations that passed the Double Mass Curve method and had R-squared values greater than 0.90. These values were used in the study. For details on the quality of rainfall data analysis using the Double Mass Curve method, the hourly accumulated rainfall data of the desired station were plotted against the average hourly accumulated rainfall of neighboring stations. If the data of the desired station coincides with the neighboring stations, the slope of the Double Mass Curve will not change significantly or will increase steadily. The R-squared analysis of the desired station's rainfall data will also be performed by comparing the hourly accumulated rainfall data of the desired station with the average hourly accumulated rainfall of neighboring stations. Based on the results of the Double Mass Curve method and an R-squared value greater than 0.90, the stations in question were considered to have passed the rain data quality assessment. The results of the hourly rainfall data quality assessment from 238 automatic ground telemetry stations, collected from January 2018 to November 2020, were examined for quality. 233 stations passed the quality assessment, while five failed. To ensure accurate rainfall assessment using weather radar data, this study will utilize rainfall data from automatic ground telemetry stations that passed the quality assessment and are not located in radar blind areas (areas within a 10-km radius of each radar station). This is because radar blind areas often underestimate rainfall. The automatic ground telemetry stations that passed the quality assessment and were used in this study are summarized in Table 1.

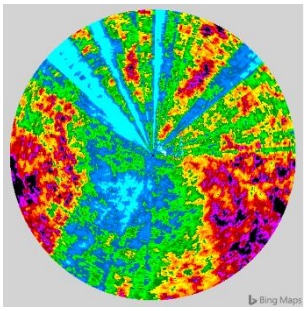

(a) Measurement angle at 0.5°

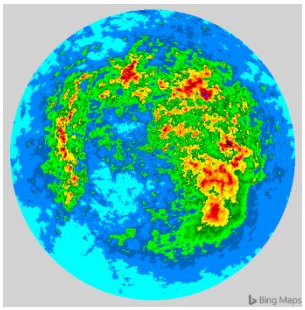

(b) Measurement angle at 1.5°

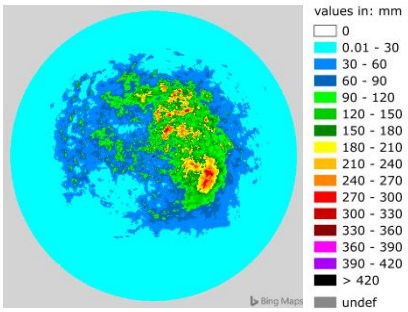

(c) Measurement angle at 2.4°

Figure 3 Sample areas of monthly accumulated rainfall measured by the Sattahip radar from three elevation angles during the July 2020 rain event

Table 1 Automatic ground telemetry stations that passed the quality assessment

Study area	Number of automatic telemetry stations			
	Passed QC	Failed QC	In radar blind area	Used in this research
Takhli radar's measuring area	124	4	1	123
Sattahip radar's measuring area	62	1	1	61
Composite measuring area of Takhli and Sattahip radar	47	-	-	47

2.2 Z-R relationship analysis

Data from 482 and 510 rainfall events within the measurement radius of the Takhli and Sattahip radars were analyzed using a regression method to determine the Z-R relationship. The principle of the regression method is to select a pair of radar reflectivity values and rainfall intensity values from a ground-based automatic telemetry station at the same location and time to analyze the Z-R relationship. The study divided rainfall events into two groups. The first group, 80% of the total rainfall events, was used for calibration. (Calibration) to analyze the Z-R relationship equation ($Z = aR^b$) [22-25] by using the data pair of the relationship between the radar reflectivity values that are more than 15 dBZ and to avoid the problem of the impact of the radar detecting the signal caused by hail, so in the case that the radar reflectivity is more than 53 dBZ, it will be considered to be equal to 53 dBZ and consider using the rain intensity value from the ground automatic telemetry station that is more than 0.2 mm/hr. to reduce the error of rain data from the ground automatic telemetry station in the case of low rain measurements at the same location and time to analyze the Z-R relationship equation ($Z = aR^b$) by considering using a constant parameter b equal to 1.6, consistent with the study [26-27] and analyzing the parameter a that makes the value (Mean Square Error, MSE) between the rain intensity values from the radar and the rain intensity from the ground automatic telemetry station have the least value. The second group is the data of the remaining 20% of the total number of rain events. The reliability of the Z-R relationship equations analyzed from the first group of data was verified. Details of the data used to determine the optimal Z-R equations for the Takhli and Sattahip radars are shown in Table 2. The optimal Z-R equations ($Z = aR^b$) for the Takhli and Sattahip radars were determined based on the RMSE statistic (as shown in Equation 1) between the rain intensity from the Takhli and Sattahip radars. The rain intensity estimated using the suggested Z-R relationship equations compared to the rain intensity from the ground-based automatic telemetry station should have the lowest value.

Table 2 Data used to determine the optimal Z-R equations for the Takhli and Sattahip radars

Radar station	Radar reflectivity data	Automatic telemetry stations	Calibration rainfall events	Verification rainfall events
Takhli radar	Elevation angle Level 2 (1.3°)	170 Stations	386 Days (Dec 25, 2018 to Feb 2, 2020)	96 Days (Mar 3 to Aug 31, 2020)
Sattahip radar	Elevation angle Level 2 (1.5°)	108 Stations	408 Days (Feb 2, 2018 to Dec 13, 2019)	102 Days (Nov 14 to Aug 31, 2020)

$$\mathrm{RMSE}=\sqrt{\frac{1}{\mathrm{N}\times \mathrm{N}_t}\sum_{\mathrm{t}=1}^{N_t}\sum_{\mathrm{i}=1}^{N}\left(R_{\mathrm{i,t}}\text{-}\mathrm{G}_{\mathrm{i,t}}\right)^2} \quad (1)$$

Where

$R_{\mathrm{i,t}}$ is the radar rainfall intensity at pixel i, estimated from the suggested (Z-R) relationship equation, in hours t (mm) with an automatic telemetry station located.

$G_{\mathrm{i,t}}$ is the rainfall intensity measured by a ground-based automatic telemetry station at pixel i, with an automatic telemetry station located, in hours t (mm).

N is the total number of pixels with an automatic telemetry station located.

N_t is the number of rain periods (h).

2.3 Analysis of radar rainfall intensity values at composite pixel locations using the Relative Weight Matrix method

Between August 22, 2018, and August 31, 2020, 267 rainfall events within the measurement radius of the Takhli and Sattahip radar composite radars were analyzed to determine rainfall intensity values at composite pixel locations of both radars using the Relative Weight Matrix method. The calculation details are as follows:

• Overlay radar rainfall intensity values at the measured pixel locations of the Takhli and Sattahip radars. This is calculated using the equation $Z = 138R^{1.6}$ of the Takhli radar, the equation $Z = 170R^{1.6}$ of the Sattahip radar, the equation $Z = 200R^{1.6}$ (Marshall and Plamer) [10], or the equation $Z = 300R^{1.4}$ (Woodley and Herndon) [28] to calculate the composite radar rainfall intensity at the aforementioned pixel location.

• Calculate the relative weight matrix of the radar used to calculate the composite radar rainfall intensity at each pixel location measured by each radar using Equation 2.

$$W_i = Q_i/Q_0 \quad (2)$$

Where

W_i is the relative weight matrix of radar i at the considered pixel location.

Q_i is the weight matrix of radar i at the considered pixel location is equal to the detection distance of radar i (240 km) minus the distance between the considered pixel locations.

Q_0 is the total weight matrix of each radar at the considered pixel location.

• Calculate the radar rainfall intensity at the pixels where the composite radar measurements overlap using Equation 3.

$$R_c = \sum_i^k W_i * \mathrm{R}_i \quad (3)$$

Where

R_c is the composite radar rain intensity value at the considered pixel location.

R_i is the radar rain intensity value of radar i at the considered pixel location.

k is the number of composite radars at the considered pixel location.

This study presents five methods for estimating radar rain intensity at composite pixels of Takhli and Sattahip radars. They include Method 1, rain intensity estimated from equation $Z = 138R^{1.6}$ for Takhli radar only; Method 2, rain intensity estimated from equation $Z = 170R^{1.6}$ for Sattahip radar only; Method 3, composite rain intensity estimated from equation $Z = 200R^{1.6}$; Method 4, composite rain intensity estimated from equation Z = 300R1.4; and Method 5, composite rain intensity estimated from equation $Z = 138R^{1.6}$ for Takhli radar combined with equation $Z = 170R^{1.6}$ for Sattahip radar, respectively. These five methods will be analyzed to find the most appropriate method for estimating radar rain intensity at composite pixels of Takhli and Sattahip radars.

The optimal method for estimating radar rainfall intensity at the composite pixel location of the Takhli and Sattahip radars, based on rainfall events from August 22, 2018, to August 31, 2020, within the radar detection range of the Takhli and Sattahip radars, totaling 267 events, was considered. The RMSE statistic, as shown in Equation (1), the MAE statistic, as shown in Equation 4, and the BIAS value, as shown in Equation 5, between the radar rainfall intensity (mm/h) estimated from all five rainfall estimation methods and the rainfall intensity from the automatic rainfall station (mm/h), must be minimal.

$$\mathrm{MAE}=\frac{1}{\mathrm{N}\times\mathrm{N}_t}\sum_{\mathrm{t}=1}^{N_t}\sum_{\mathrm{i}=1}^{N}\left|R_{\mathrm{i,t}}\text{-}\mathrm{G}_{\mathrm{i,t}}\right| \quad (4)$$

$$\mathrm{BIAS}=\frac{1}{\mathrm{N}\times\mathrm{N}_t}\sum_{\mathrm{t}=1}^{N_t}\sum_{\mathrm{i}=1}^{N}R_{\mathrm{i,t}}\text{-}\mathrm{G}_{\mathrm{i,t}} \quad (5)$$

Where

$R_{\mathrm{i,t}}$ is the radar rainfall intensity at pixel i, estimated from the suggested Z-R relationship equation in hour t (mm) with the automatic telemetry station.

$G_{\mathrm{i,t}}$ is the rainfall intensity measured from the ground-based automatic telemetry station at pixel i. where automatic telemetry stations are located in hours t (mm)

N is the total number of pixels where automatic telemetry stations are located

N_t is the number of rainy periods (h)

3. Results and discussion

3.1 Z-R relationship analysis

The results of the analysis of the optimal Z-R relationship equation for the Takhli radar at the second (1.3°) measurement angle were $Z = 138R^{1.6}$, with the estimated rainfall intensity being closer to that measured by the ground-based automatic telemetry station than to that measured using the equations $Z = 200R^{1.6}$ (Marshall and Plamer) [10] and $Z = 300R^{1.4}$ (Woodley and Herndon) [28]. Considering the RMSE values shown in Table 3, it was found that the RMSE values for the rainfall intensity estimated using the equation $Z = 138R^{1.6}$ were lower than those measured using the equations $Z = 200R^{1.6}$ and $Z = 300R^{1.4}$, respectively.

The results of the analysis of the optimal Z-R relationship equation for the Sattahip radar at the second (1.5°) measurement angle were $Z = 170R^{1.6}$, with the estimated rainfall intensity being closer to that measured by the ground-based automatic telemetry station than to that measured using the equation $Z = 200R^{1.6}$ (Marshall and Plamer) [10] and $Z = 300R^{1.4}$ (Woodley and Herndon) [28] and when considering the RMSE values as shown in Table 4, it was found that the RMSE values for the rainfall intensity estimated using the equation $Z = 170R^{1.6}$ were less than the rainfall intensity estimated using the equations $Z = 200R^{1.6}$ and $Z = 300R^{1.4}$, respectively.

Table 3 RMSE values for rainfall estimates using equations $Z = 138R^{1.6}$, $Z = 200R^{1.6}$, and $Z = 300R^{1.4}$ from Takhli radar data at a 1.3° measurement angle

Rainfall event	RMSE (mm/h)		
	$Z = 138R^{1.6}$	**$Z = 200R^{1.6}$**	**$Z = 300R^{1.4}$**
Calibration (386 days) (Dec 25, 2018 to Feb 2, 2020)	4.459	4.542	4.604
Verification (96 days) (Mar 3 to Aug 31, 2020)	5.675	5.875	5.928

Table 4 RMSE values for rainfall estimates using equations $Z = 170R^{1.6}$, $Z = 200R^{1.6}$, and $Z = 300R^{1.4}$ from Sattahip radar data at a 1.5° measurement angle

Rainfall event	RMSE (mm/h)		
	$Z = 170R^{1.6}$	**$Z = 200R^{1.6}$**	**$Z = 300R^{1.4}$**
Calibration (408 days) (Feb 2, 2018 to Dec 13, 2019)	4.151	4.170	4.219
Verification (102 days) (Nov 14, 2019 to Aug 31, 2020)	4.286	4.290	4.358

3.2 Analyze and identify the most appropriate method for estimating radar rainfall intensity at the composite pixel location of the Takhli and Sattahip radars.

The results of the RMSE, MAE, and BIAS statistics of the five radar rainfall intensity estimation methods at the composite pixel location of the Takhli and Sattahip radars compared to rainfall intensity from ground-based automatic rain gauge stations (mm/h) are shown in Figures 4-6.

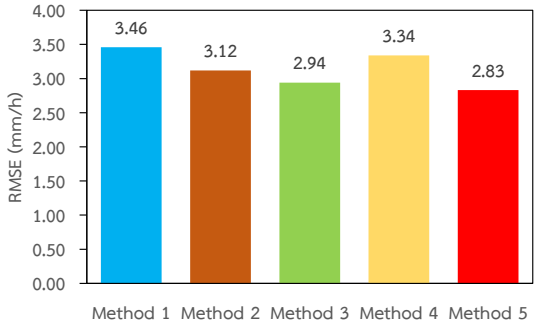

Figure 4 RMSE statistics of the five radar rainfall intensity estimation methods compared to rainfall intensity from the automatic rain gauge station

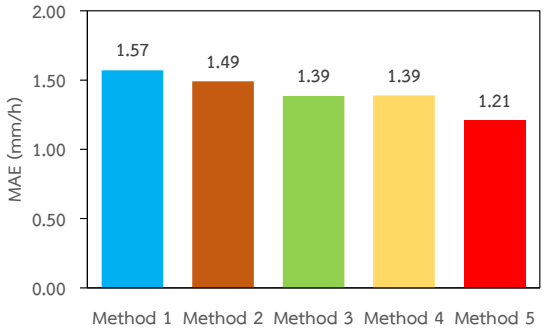

Figure 5 MAE statistics of the five radar rainfall intensity estimation methods compared to rainfall intensity from the automatic rain gauge station

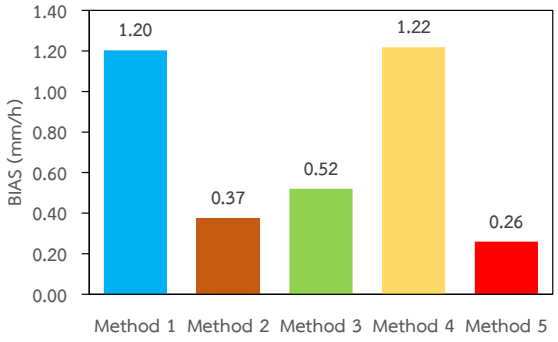

Figure 6 BIAS statistics of the five radar rainfall intensity estimation methods compared to rainfall intensity from the automatic rain gauge station

It was shown that, considering the RMSE, MAE, and BIAS statistics, the fifth composite rainfall intensity estimation method, which uses the equation $Z = 138R^{1.6}$ for the Takhli radar and the equation $Z = 170R^{1.6}$ for the Sattahip radar, has the highest accuracy in estimating rainfall intensity compared to methods 3, 2, 4, and 1. This result is consistent with studies [29-33] that stated that when estimating radar rainfall intensity at composite pixels located far from the Takhli and Sattahip radar stations, when estimating rainfall intensity using Method 1, which uses the equation $Z = 138R^{1.6}$ for the Takhli radar alone, and Method 2, which uses the equation $Z = 170R^{1.6}$ for the Sattahip radar alone, there are still remaining errors due to the influence of the earth's curvature and the increase in radar beamwidth with distance. Therefore, when using the composite rain intensity values estimated from rain intensity assessment methods 5, 3 and 4, it will help increase the accuracy of radar rain intensity assessment at the composite pixel location of Takhli radar and Sattahip radar [34-41] because it can help reduce the error of reflectivity values in rain measurements from Takhli radar and Sattahip radar due to the influence of the curvature of the earth and the increase of radar beam width with distance, respectively.

4. Conclusions

1) Composite rainfall intensity values estimated using Methods 5, 3, and 4 will increase the accuracy of radar rainfall intensity estimates at composite pixels of the Takhli and Sattahip radars, compared to rainfall intensity estimates using Method 1, which estimates

rainfall intensity using the equation $Z = 138R^{1.6}$ for the Takhli radar alone, or Method 2, which estimates rainfall intensity using the equation $Z = 170R^{1.6}$ for the Sattahip radar alone. This is because it can help reduce the error in the reflectivity of rain measurements from the Takhli and Sattahip radars due to the influence of the Earth's curvature and the increase in radar beamwidth with distance.

2) The composite rain intensity values estimated using Method 5, when compared to the rain intensity estimated using Methods 1-4, can increase the accuracy of rain estimates by 22.26%, 10.25%, 3.89%, and 18.02%, respectively. The MAE can increase the accuracy of rain estimates by 29.75%, 23.14%, 14.88%, and 14.88%, respectively. The BIAS can increase the accuracy of rain estimates by 361.54%, 42.31%, 100.00%, and 369.23%, respectively.

5. Acknowledgements

This study would like to thank the Royal Rainmaking and Agricultural Aviation Department for providing the Takhli and Sattahip radar reflectivity data stored in volume files, and the Hydro-Informatics Institute (Public Organization) for providing hourly rainfall data from the ground-based automated telemetry station and providing various assistance during the study.

6. References

[1] Morin E, Gabella M. Radar-based quantitative precipitation estimation over Mediterranean and dry climate regimes. J Geophys Res. 2007;112:D20108. https://doi.org/10.1029/2006JD008206.

[2] Einfalt T, Arnbjergnielsen K, Golz C, Jensen N, Quirmbach M, Vaes G, Vieux B. Towards a roadmap for use of radar rainfall data in urban drainage. J Hydrol. 2004;299(3-4):186–202. https://doi.org/10.1016/S0022-1694(04)00365-8.

[3] Gires A, Tchiguirinskaia I, Schertzer D, Schellart A, Berne A, Lovejoy S. Influence of small scale rainfall variability on standard comparison tools between radar and rain gauge data. Atmos Res. 2014;138:125–38. https://doi.org/10.1016/j.atmosres.2013.11.008.

[4] Hou J, Wang NA, Guo K, Li D, Jing H, Wang T, Hinkelmann R. Effects of the temporal resolution of storm data on numerical simulations of urban flood inundation. J Hydrol. 2020;589:125100. https://doi.org/10.1016/j.jhydrol.2020.125100.

[5] Ochoa-Rodriguez S, Wang LP, Gires A, Pina RD, Reinoso-Rondinel R, Bruni G, Ichiba A, Gaitan S, Cristiano E, van Assel J, Kroll S, Murl`a-Tuyls D, Tisserand B, Schertzer D, Tchiguirinskaia I, Onof C, Willems P. Veldhuis MC. Impact of spatial and temporal resolution of rainfall inputs on urban hydrodynamic modelling outputs: A multi-catchment investigation. J Hydrol. 2015;531:389–407. https://doi.org/10.1016/j.jhydrol.2015.05.035.

[6] Thorndahl S, Einfalt T, Willems P, Nielsen JE, ten Veldhuis MC, Arnbjerg-Nielsen K, Rasmussen MR, Molnar P. Weather radar rainfall data in urban hydrology. Hydrol Earth Syst Sci. 2017;21(3):1359–80. https://doi.org/10.5194/hess-21-1359-2017.

[7] Kumjian MR. Principles and applications of dual-polarization weather radar. Part I: Description of the polarimetric radar variables. J Oper Meteorol. 2013;1(19):226–42. https://doi.org/10.15191/nwajom.2013.0119.

[8] Kaiser M, Günnemann S, Disse M. Spatiotemporal analysis of heavy rain-induced flood occurrences in Germany using a novel event database approach. J Hydrol. 2021;595:125985. https://doi.org/10.1016/j.jhydrol.2021.125985.

[9] Mobini S, Nilsson E, Persson A, Becker P, Larsson R. Analysis of pluvial flood damage costs in residential buildings–A case study in Malmo. Int J Disaster Risk Reduct. 2021;62:102407. https://doi.org/10.1016/j.ijdrr.2021.102407.

[10] Marshall J S, Palmer WMK. The Distribution of raindrops with size. Journal of Meteorology. 1984;5(4):165-6. https://doi.org/10.1175/1520-0469(1948)005<0165:TDORWS>2.0.CO;2.

[11] Mapiam PP, Sriwongsitanon N. Climatological Z-R relationship for radar rainfall estimation in the upper Ping river basin. ScienceAsia. 2008;34:215-22. https://doi.org/10.2306/scienceasia1513-1874.2008.34.215.

[12] Hanchoowong R, Weesakul U, Chumchean S. Bias correction of radar rainfall estimates based on a geostatistical technique. ScienceAsia. 2012;38:373-85. https://doi.org/10.2306/scienceasia1513-1874.2012.38.373.

[13] Chantraket P, Detyothin C, Pankaew S. Kirtsaeng S. An operational weather radar-based calibration of Z–R relationship over Central Region of Thailand. Int J Eng. 2016;2:92–100.

[14] Wang LP, Ochoa-Rodríguez S, Van Assel J, Pina RD, Pessemier M, Kroll S, Willems P, Onof C. Enhancement of radar rainfall estimates for urban hydrology through optical flow temporal interpolation and Bayesian gauge based adjustment. J Hydrol. 2015; 531:408-26. https://doi.org/10.1016/j.jhydrol.2015.05.049.

[15] Hanchoowong R. Analysis of the Z-R equation for use in estimating rainfall of the Takhli radar. Journal of Engineering and Innovation. 2022;15(4):172-83.

[16] Michelson D, Einfalt T, Holleman I, Gjertsen U, Friedrich K, Haase G, Lindskog M, Sztuc, J. Weather radar data quality in Europe: Quality control and characterization, COST 717 Working Document WDF_20_200204_1. 2004.

[17] Hydro & meteo GmbH & Co. KG. SCOUT Documentation Version 3.32. Hydro & meteo GmbH & Co. KG., Germany. 2016.

[18] Battan LJ. Radar observation of the atmosphere. The University of Chicago Press. 1973:324.

[19] Chumchean S. Improved estimation of radar rainfall for use in hydrological modelling. Ph.D. Thesis, University of New South Wales, Sydney, Australia. 2004.

[20] Delrieu G, Andrieu H, Creutin JD. Quantification of path-integrated attenuation for X-and C-band weather radar systems operating in Mediterranean heavy rainfall. J Appl Meteor. 2000;39(6):840-50. https://doi.org/10.1175/1520-0450(2000)039<0840:QOPIAF>2.0.CO;2.

[21] Futon RA, Breidenbach JP, Seo DJ, Miller DA, O'Brannon T. The WSD–88D rainfall algorithm. Weather Forecasting. 1998;13: 377-95. https://doi.org/10.1175/1520-0434(1998)013<0377:TWRA>2.0.CO;2.

[22] Austin PM. Relation between measured radar reflectivity and surface rainfall. Monthly Weather 520 Review. 1987;115:1053-70. https://doi.org/10.1175/1520-0493(1987)115<1053:RBMRRA>2.0.CO;2.

[23] Williams CR, Ecklund WL, Gage KS. Classification of precipitating clouds in the tropics using 915-MHz wind profilers. J Atmos Oceanic Technol. 1995;12(5):996-1012. https://doi.org/10.1175/1520-0426(1995)012<0996:COPCIT>2.0.CO;2.

[24] Atlas D, Ulbrich CW, Marks Jr FD, Amitai E, Williams CR. Systematic variation of drop size and radar-rainfall relations. J Geophys Res. 1999;104(D6):6155-69. https://doi.org/10.1029/1998JD200098.

[25] Harrison DL, Driscoll SJ, Kitchen M. Improving precipitation estimates from weather radar using quality control and correction techniques. Meteorol Appl. 2000;6:135–44. https://doi.org/10.1017/S1350482700001468.
[26] Mapiam P, Sriwongsitanon N, Chumchean S, Sharma A. Effects of rain gauge temporal resolution on the specification of a Z-R relationship. J Atmos Oceanic Technol. 2009;26:1302-14. https://doi.org/10.1175/2009JTECHA1161.1.
[27] Mapiam P, Sharma A, Sriwongsitanon N. Defining the Z–R relationship using gauge rainfall with coarse temporal resolution: implications for flood forecasting. J Hydrol Eng. 2014;19(8):04114003. https://doi.org/10.1061/(ASCE)HE.1943-5584.0000616.
[28] Woodley W, Herndon A. A raingage evaluation of the Miami reflectivity-rainfall rate relation. J Appl Meteor. 1970;9(2):258-64. https://doi.org/10.1175/1520-0450(1970)009<0258:AREOTM>2.0.CO;2.
[29] Kitchen M, Brown R, Davies AG. Real-time correction of weather radar data for the effects of bright band, range and orographic growth in widespread precipitation. QJ Roy Meteorol Soc. 1994;120:1231-54. https://doi.org/10.1256/smsqj.51905.
[30] Seo DJ. Real-time estimation of rainfall fields using radar rainfall and rain gage data. J Hydrol. 1998;208:37–52. https://doi.org/10.1016/S0022-1694(98)00141-3.
[31] Chumchean S, Sharma A, Seed A. An integrated approach to error correction for real-time radar-rainfall estimation. J Atmos Ocean Tech. 2006;23:67–79. https://doi.org/10.1175/JTECH1832.1.
[32] Rabiei E, Haberlandt U. Applying bias correction for merging rain gauge and radar data. J Hydrol. 2015;522:544-57. https://doi.org/10.1016/j.jhydrol.2015.01.020.
[33] Kim J, Yoo C. Using extended Kalman filter for real-time decision of parameters of Z-R relationship. Journal of Korea Water Resources Association. 2014;47(2). https://doi.org/10.3741/JKWRA.2014.47.2.119.
[34] Einfalt T, Lobbrecht A, Leung K, Lempio G. Preparation and evaluation of a Dutch-German radar composite to enhance precipitation information in border areas. J Hydrol Eng. 2012;18(2). https://doi.org/10.1061/(ASCE)HE.1943-5584.0000649.
[35] Einfalt T, Lobbrecht A. Compositing international radar data using a weight-based scheme. Weather Radar and Hydrology. Proceedings of a symposium held in Exeter, UK, April 2011. IAHS Publ. 2012;351:20-5.
[36] Jurczyk A, Szturc J, Osródka K. Quality-based compositing of weather radar derived precipitation. QJ Roy Meteorol Soc. 2020;17(1):1-14. https://doi.org/10.1002/met.1812.
[37] Lempio G, Einfalt T, Lobbrecht A. Considerations for compositing radar data from three countries. Weather Radar and Hydrology ERAD 2012 - The Seventh European Conference on Radar in Meteology and Hydrology, ERAD 2012. 2012.
[38] Nielsen JE, Thorndahl S, Rasmussen MR. Improving weather radar precipitation estimates by combining two types of radars. Atmos Res. 2014;139:36-45. https://doi.org/10.1016/j.atmosres.2013.12.013.
[39] Lengfeld K, Clemens M, Münster H, Ament F. Performance of high-resolution X-band weather radar networks–the PATTERN example. Atmos. Meas. Tech. 2014;7(12):4151–66. https://doi.org/10.5194/amt-7-4151-2014.
[40] Lengfeld K, Clemens M, Merker C, Münster H, Ament F. A simple method for attenuation correction in local X-band radar measurements using C-band radar data. J Atmos Oceanic Tech. 2016;33(11):2315–29. https://doi.org/10.1175/JTECH-D-15-0091.1.
[41] Hosseini SH, Hashemi H, Berndtsson R, South N, Aspegren H, Larsson R, Olsson J, Persson A, Olsson L. Evaluation of a new X-band weather radar for operational use in south Sweden. Water Sci Technol. 2020;81(8):1623–35. https://doi.org/10.2166/wst.2020.066